Peptidylarginine deiminase is involved in maintaining the cornified oral mucosa of rats

Seiichi Arita[1], Mitsutoki Hatta[2], Kunitoshi Uchida[2], Tomo Kita[2], Kazuhiko Okamura[3], Takanori Ryu[1], Hiroshi Murakami[1], Ryuji Sakagami[1], and Jun Yamazaki[2*]

[1] Department of Odontology, [2] Department of Physiological Science & Molecular Biology, and [3] Department of Morphological Biology, Fukuoka Dental College, 2-15-1 Tamura, Sawara-ku, Fukuoka 814-0193, Japan

Keywords: peptidylarginine deiminase, epithelium, oral mucosa, filaggrin

Running title: Peptidylarginine deiminase in oral mucosa

*Corresponding author: Jun Yamazaki, PhD, Department of Physiological Science & Molecular Biology, Fukuoka Dental College, 2-15-1 Tamura, Sawara-ku, Fukuoka 814-0193, Japan. Tel. 81-92-801-0411 ext. 669; Fax: 81-92-801-4909; E-mail: junyama@college.fdcnet.ac.jp

Abstract

Background and Objective: Epithelial cells derived from different regions exhibit marked differences in their differentiation capacity, allowing them to provide a suitable protective barrier. We aimed to clarify the role of peptidylarginine deiminase (PAD) in modifying the key epidermal proteins filaggrin (FLG) and keratin 1 (K1) during stratification of the rat palate and buccal mucosa.

Materials and Methods: We performed immunofluorescence, immunoblotting, PAD activity assays, and two-dimensional electrophoresis, and developed an organotypic culture model.

Results: PAD1 expression was highest in the palate, whereas PAD2, PAD3, and PAD4 expression was highest in the skin, suggesting the tissue-specific expression of PAD isozymes that leads to differences in calcium dependency. Immunoblotting showed that the FLG monomer, as well as its degradation products and precursor (proFLG), were most abundantly expressed in the skin but had low expression in the palate, whereas only faint proFLG expression was detected in the buccal mucosa. FLG and K1 were co-localized with PAD1 and were likely to be citrullinated in the cornified layers of the skin; this co-localization was not detected on the palatal surface, and dot-like presence of proFLG that might be citrullinated and that of PAD1 were found in the granules of the palate. Organotypic models derived from the rat palate revealed that PAD inhibition reduced the breakdown of FLG, increased its association with K1 together with epithelial compaction, and decreased permeability in a dye permeability assay. Conversely, PAD stimulation had the opposite effects.

Conclusions: Citrullination is likely a protein modification that plays an important role in maintaining the structure and function of oral cornified mucosa in a way that is distinctly different from that of the skin.

Introduction

Citrullination or deimination is one of the post-translational modifications of proteins. In this process, peptidylarginine deiminase (PAD) changes the structure of key epidermal proteins, such as filaggrin (FLG) and keratins, by converting arginine residues into neutral citrulline residues in the stratifying epithelium (1). Profilaggrin (ProFLG) is a large molecule that accumulates in keratohyalin granules. During cornification of the skin, it is proteolyzed into FLG repeats (monomers) and other domains (2). FLG monomers bind to keratin intermediate filaments (KIFs), causing tight aggregation into macrofibrils (3). The tightly packed KIF leads to cellular compaction aligned parallel to the outer surface of the epidermis, which generates a barrier against the environment (4). However, loss of positive charge per citrulline residue induced by PAD changes the intramolecular and intermolecular interactions with the keratin matrix, making the less ordered FLG structure more susceptible to proteolytic degradation (1).

The PAD family is composed of five calcium-dependent isozymes. PAD1 has mainly been detected in the human epidermis and uterus (1), and rat epidermis and stomach (5). Rat PAD1 cDNA was cloned from a retinoic acid-treated culture of a newborn keratinocyte cell line (6). PAD1 plays a major role in the citrullination of keratin 1 (K1) in the epidermis (7, 8). K1 citrullination was shown to be decreased in the hyperproliferative plaques in psoriasis and bullous congenital ichthyosiform erythroderma (9, 10). PAD2 is expressed in a variety of rat tissues such as the epidermis, brain, lung, spleen, stomach, and uterus (5). PAD3 is expressed in the inner root sheath and medulla of hair follicles where it crosslinks the structural protein trichohyalin (1, 11). PAD4 is found in hematopoetic cells (1). All of these PAD subtypes are reportedly expressed in the rat epidermis (5). Among them, PAD1 and PAD3 proteins are

colocalized with FLG, suggesting that they are both involved in FLG citrullination in the epidermis (8, 11).

Epithelial cells derived from different regions including the oral mucosa exhibit marked differences in their differentiation capacity, allowing them to provide a suitable protective barrier (12). Dale *et al.* (13) demonstrated site and age differences in the distribution of FLG and its precursor protein in rat oral mucosa; as in the epidermis, the protein was observed in cornified layers and in keratohyalin granules throughout the mouth of newborn (0–2 days old) rats, whereas it was mainly present in keratohyalin granules in adult rats. Our previous immunohistochemical and real-time PCR studies showed that the relative levels of FLG differed among the palate, buccal mucosa, esophagus, and skin in 7-day-old rats (14). FLG is expressed in the human oral mucosa as well as in the epidermis (15, 16). ProFLG is detectable in human nonkeratinized, parakeratinized, and orthokeratinized oral epithelium, although FLG monomer is expressed in only the orthokeratinized palate (15). Expression of FLG proteins in the human oral mucosa was shown to markedly increase under pathological conditions involving hyperkeratosis such as lichen planus and leucoplakia (17), which occur independently of defects in the FLG gene (18). These data suggest that the enzymatic breakdown of proFLG and the resulting pattern of stratification are likely to be distinct among stratified tissues such as the skin and oral mucosa. Thus, it is likely that the post-translational modification of proFLG and FLG by PAD influences epithelial differentiation and cornification of oral mucosa (15).

In this study, we aimed to clarify the role of protein citrullination in the stratification and cornification of oral mucosa. First, we compared the expression of FLG, proFLG, and PAD isozymes, and evaluated PAD activity and protein citrullination in the epithelial cell layers of the skin, palate, and buccal mucosa of 7-

day-old rats. Second, we developed a 3-dimensional (3D) mucosal model derived from epithelial cells and fibroblasts isolated from the rat palate. Finally, we examined whether an inhibitor and activator of PAD could alter FLG expression, as well as the structure and function of the epithelial layers.

Materials and Methods

Antibodies and reagents

The following primary antibodies were used: mouse monoclonal K1 (NB100-2756; Novus Biologicals, Littleton, CO), β-actin (sc-47778; Santa Cruz Biotechnology, Santa Cruz, CA), rabbit polyclonal anti-cyclic citrullinated peptide (CCP, bs-1053R; Bioss Inc., Woburn, MA), anti-PAD1 (NBP2-37761; Novus Biologicals), human anti-modified citrulline (MC, clone C4; EMD Millipore Corp., Temecula, CA), and rabbit anti-FLG antiserum (generously gifted by Dr. Ishigami, Tokyo Metropolitan Institute of Gerontology, Tokyo, Japan). Cl-Amidine trifluoroacetate salt was purchased from Cayman Chemical (Ann Arbor, MI) and theophylline-7-acetic acid (acefylline) was purchased from Toronto Research Chemicals, Inc. (North York, Canada). The other compounds were obtained from Sigma-Aldrich (St. Louis, MO).

Histological and immunohistochemical examination

Neonatal Wistar rats (7 days old) were anesthetized with isoflulane and sacrificed. Permission for the procedures was granted by the Animal Research Committee of Fukuoka Dental College (Fukuoka, Japan). The palate, buccal mucosa, and abdominal skin were dissected as previously described (14). The *in vivo* rat tissues or reconstructed model were fixed in 10% formalin solution, routinely processed, and embedded in paraffin. Sections 3 μm thick were stained with hematoxylin and eosin (H&E). To

obtain frozen sections 10 μm thick, the samples were fixed briefly in 4% paraformaldehyde (PFA) solution, gradually dehydrated with 10%, 15%, and 20% sucrose solution, and embedded in Super Cryoembedding Medium (Section-Lab Co., Hiroshima, Japan). To detect MC immunoreactivity in the tissue sections, citrulline residues on the sections were chemically modified with 2,3-butanedione monoxime and antipyrine under acidic conditions (19) prior to applying the antibodies. For immunofluorescence double staining, the tissue sections with or without chemical modification were blocked in 10% normal goat serum and then incubated with a combination of two antibodies listed below for 2 h; anti-FLG serum (1:40,000), anti-MC (1:100), CCP (1:200), PAD1 (1:100), and K1 (1:100) antibodies, followed by a 1 h incubation at room temperature with goat anti-rabbit, anti-mouse, or anti-human immunoglobulin G (IgG) antibodies conjugated with Alexa 488 or Alexa 594 (1:800). The sections were counterstained with DAPI (ProLong Gold; Thermo Fisher Scientific, Waltham, MA). Fluorescence was observed using a fluorescence microscope (BZ-9000; Keyence, Osaka, Japan) and a confocal laser scanning microscope (LSM710; Carl Zeiss MicroImaging GmbH, Gottingen, Germany). Quantification of the relative area and width of the layers in the images and calculation of Pearson's colocalization coefficient were performed with ImageJ software (National Institutes of Health [NIH], Bethesda, MD).

Evaluation of mRNA expression levels by real-time PCR

Total RNA was isolated from the rat tissues and the reconstructed model (NucleoSpin RNA Kit; Macherey-Nagel GmbH & Co. KG, Düren, Germany), after which the cDNA was reverse transcribed (PrimeScript RT Reagent Kit; Takara Bio Inc., Tokyo, Japan). Quantitative PCR (qPCR) was performed with the Applied Biosystems

7500 Real-Time PCR System with the thermal cycling conditions recommended by the manufacturer, and with the SYBR^{R} Green method using a pair of specific primers to target rat proFLG (Forward: 5′-ATGCTAGATGTGGACCACGATGAC-3′, Reverse: 5′-TGTTCCCTCTTCCTCTTGGGCTT-3′; GenBank accession number: XM_003753631), rat PAD1 (Forward: 5′-CACAGGCAAGGTGAAGAAAGG-3′, Reverse: 5′-TGTTTGTAGTTGGAGAGGGAGG-3′; GenBank accession number: NM_019332.1), rat PAD2 (Forward: 5′-TCCTGAAAGAGGTGAAGAACCTG-3′, Reverse: 5′-TACTGGGAAGCCTTTGTGAGG-3′; GenBank accession number: NM_017226.1), rat PAD3 (Forward: 5′-TTGGCTTGTGCTTCCTATGGT-3′, Reverse: 5′-GTAGTGAGGGTGTGAAATAGTCTG-3′; GenBank accession number: NM_017230.2) and rat PAD4 (Forward: 5′-GCTGGGAAGGATCAGAGCAC-3′, Reverse: 5′-GGGAGTCTTCGTGCTTAGGG-3′; GenBank accession number: NM_017227.1). The qPCR reactions were performed in duplicate. A standard curve was used to calculate expression of the PADs and proFLG normalized to rat GAPDH, which served as the endogenous control (Forward: 5′-GACATGCCGCCTGGAGAAAC-3′, Reverse: 5′-AGCCCAGGATGCCCTTTAGT-3′; GenBank accession number: NM_017008), and the relative quantity was compared.

Gel electrophoresis and western blot analysis

The rat oral mucosa was minced and homogenized in lysis buffer containing 8 M urea, 10 mM EDTA, 1 mM dithiothreitol (DTT), 50 mM Tris-HCl (pH 8.0), and 1% protease inhibitor cocktail (Sigma). After extraction, the lysates (15 μg) were centrifuged for 5 min at 1000 × g, and the proteins were resolved on gradient sodium dodecyl sulfate-polyacrylamide gel electrophoresis (SDS-PAGE) gels (4-20%). For two-dimensional (2D) gel electrophoresis, the proteins (50–80 μg) were extracted with

lysis buffer containing 8 M urea, 2 M thiourea, 2% CHAPS, 1% Triton X-100, 2% Biolyte (pH 4–10; BioRad, Hercules, CA), 10 mg/mL DTT, 1% protease inhibitor cocktail, and 10 mM Tris-Cl (pH 8.0). Proteins were loaded on agarose gels with a pH range of 3–10 (A-M310, agarGEL; ATTO Corp., Tokyo, Japan), separated in the first dimension using non-equilibrium pH gradient electrophoresis (NEpHGE) (20), and separated on SDS-PAGE gradient gels (4–20%). Then the samples were electrophoretically transferred to a PVDF membrane (Hybond-P; GE Healthcare, Wauwatosa, WI). Total protein staining was performed using colloidal gold solution (ProtoGold; Agar Scientific, Essex, UK). To detect MC proteins, citrulline residues on the membrane were modified with 2,3-butanedion monoxime and antipyrine by overnight incubation under acidic conditions (Anti-Citrulline [Modified) Detection Kit, 17-347B; EMD Millipore). For protein detection, membranes were incubated with anti-FLG serum (1:100,000), and anti-MC (1:1000), CCP (1:500), β-actin (1:1000), and K1 (1:100), antibodies followed by incubation with horseradish peroxidase (HRP)-conjugated goat anti-rabbit and anti-mouse IgG antibodies (1:400,000; Jackson ImmunoResearch, West Grove, PA), and goat anti-human IgG (1:2000, EMD Millipore). For stripping of immunoblots, membrane was incubated with 62.5 mM Tris buffer (pH=6.7) containing 100 mM 2-mercaptoethanol and 2% SDS at 37 ºC for 15 min. Proteins were visualized using enhanced chemiluminescence (ImmunoStar LD; Wako Pure Chemical, Osaka, Japan).

PAD activity

An antibody-based assay for PAD activity (ABAP assay) was performed to measure PAD activity (21) (MQ17.101-96, ModiQuest Research, Nijmegen, The Netherlands). Briefly, tissue samples were homogenized in lysis buffer (100 mM NaCl, 10 mM β-

mercaptoethanol, 10% glycerol, 1% protease inhibitor cocktail, 20 mM Tris-HCl pH 7.4). After centrifugation at 4°C, the tissue supernatant (1 μg total protein) or blank supernatant diluted in citrullination buffer containing different concentrations of calcium was incubated at 37°C for 75 min in the wells in which arginine-containing peptides were immobilized. Immobilized peptides containing citrulline were used as a positive control. PAD activity was assayed using a specific monoclonal mouse antibody for citrulline, HRP-labeled anti-mouse IgG antibody, and tetramethylbenzidine substrate, followed by measurement of optical density at 450 nm (OD_{450}) in a microplate reader (1420 ARVO MX; Perkin Elmer Inc., Waltham, MA). Specific PAD activity in several tissue types was calculated using a regression line of the relationship between the measured OD_{450} values and the known activities (0.012–3 mU) of human recombinant PAD4 (hPAD4) on a semi-log scale.

Reconstruction of a rat oral mucosal model using collagen gel matrix culture

Oral mucosa was obtained from the palatal and buccal regions of 7-day-old Wistar rats. All procedures were conducted based on previous studies on oral mucosa (14, 22, 23). Epithelium and lamina propria were separated from the mucosa after incubation with dispase. The latter was minced into pieces and cultured in Dulbecco's Modified Eagle Medium (DMEM) containing 10% fetal bovine serum (FBS). After fibroblasts were sprouted from the tissue, the cells were cultured in new medium for 5–6 days, followed by one round of subculturing. A total of 3 mL type I collagen gel was mixed with 2×10^6 fibroblast cells, and poured onto a cell culture insert (2.5 cm diameter, Millicell CM; Millipore) as previously described (14). After digestion of the epithelial tissue with trypsin, the cells were suspended in MCDB-153 media (Kinousei Peptide Institute, Yamagata, Japan) and then overlaid on the collagen gel. The culture insert was

placed in an outer dish containing MCDB-153 + DMEM medium (1:1) supplemented with additives as previously reported (14), and incubated at 37ºC, 5% CO_2. After the epithelial cells grew to confluency, the cells on the gel surface were cultured at an air–liquid interface (airlift) by removing the medium from the cell culture insert and replacing the medium in the outer dish with DMEM supplemented with 10% FBS and growth factors in the presence of Cl-amidine, acefylline or vehicle (0.1% dimethyl sulfoxide) as a control.

To analyze permeability of the oral mucosal model, 200 μL of 1 M Lucifer yellow CH dilithium salt solution (Sigma) was added to the surface of the model. After incubation at 37°C for 10 h, the model was fixed in 4% PFA and embedded in paraffin. The sections were examined under a fluorescence microscope, and the fluorescence intensity within the non-cornified epithelial area was quantified using ImageJ software (NIH). The permeability index was calculated by dividing the intensity by the non-cornified area.

Statistics

All values are presented as the mean ± standard error of the mean. Statistical analysis was performed using one-way analysis of variance followed by a *post hoc* test. P values less than 0.05 were considered statistically significant.

Results

Expression and degradation of FLG and proFLG in rat stratified epithelial tissues

We performed histological examination of the skin, palate, and buccal mucosa from 7-day-old rats by H&E staining (Fig. 1A). In the skin, interfollicular keratinocytes were well flattened within the granular layers, and dot-like staining of the keratohyalin

granules was observed. In the palate, squamous epithelial cells and fewer granules were observed. The buccal mucosa possessed thick layers with poor cornification where the cells exhibited minimal flattening and contained granules.

Initially, we confirmed that positive staining was not observed without using the primary antibodies and antiserum employed in the present study (data not shown). Previously, Senshu *et al.* (19) demonstrated that the anti-FLG antiserum they raised was capable of detecting rat FLG precursors and breakdown products as well as FLG monomers. Fluorescence microscopy showed that the same antiserum exhibited intense immunofluorescence in the lower cornified layer of 7-day-old rat skin (Fig. 1A). The immunoreactivity faded towards the superficial part of the cornified layer. The presence of many stained nodules with obscured outlines in the granular layer indicated the notable presence of proFLG in the keratohyalin granules. In the palate, continuous staining was barely detected in the mucosal layers, although punctuate staining was visible throughout the granular layer, suggesting the presence of proFLG. Faint granular immunoreactivity was observed in the buccal mucosa. Figure 1B shows the quantitative analysis of FLG and proFLG immunofluorescence from four preparations. The relative values of the immunoreactive areas were statistically different among the three tissues in the descending order of skin > palate $\geq$ buccal mucosa.

Figure 1C shows the immunoblot profiles obtained after probing with anti-FLG antiserum. The major band located at 48 kDa from skin samples represented the FLG monomer, as previously identified (19). Additional bands were also noted below 40 kDa, representing the degradation products of FLG. Diffuse signals in the upper part of the lane probably represent high molecular weight precursors of FLG, such as proFLG (~400 kDa) and its processing intermediates including FLG dimers. In contrast, the FLG monomer and its high molecular weight precursor were less intensely stained in

palate samples, and only a faint proFLG signal was detected in the upper part of the lane of the buccal mucosa samples.

Expression and activity of PAD in stratified rat epithelial tissues

To investigate the expression of PAD isozymes in rat skin and oral mucosal tissues, we performed qPCR and immunoblot experiments. First, representative amplification of cDNA with specific primers showed that PAD1, 2, 3, and 4 and proFLG were expressed in the three types of epithelial tissues or whole skin as a control (Fig. 2A). PCR analysis demonstrated that the mRNA levels of proFLG, a major substrate of the PADs, were expressed in descending order of skin >> palate > buccal mucosa (Fig. 2B), consistent with the expression of FLG protein. We used qPCR to examine the mRNA levels of PAD1, PAD2, PAD3, and PAD4 in the epithelial layers (Fig. 2C). Both PAD2 and PAD4 mRNA was expressed in descending order of skin >> palate = buccal mucosa, whereas PAD1 mRNA expression was highest in the palate (Fig. 2C). PAD3 mRNA was present at very low levels in oral tissues relative to the skin.

The ABAP assay was performed in 5 mM calcium-containing deimination buffer. The specific activity of PAD in the epithelial layers was highest in the skin, next highest in the palate, and lowest in the buccal mucosa (Fig. 2D). We assayed PAD activity in different calcium conditions as each PAD isozyme reportedly has distinct calcium dependency. Interestingly, in the presence of 10 μM calcium, PAD activity was highest in the palatal mucosa of the three tissues, and mirrored PAD1 mRNA expression. In the presence of 100 μM calcium, PAD activity was the same in the skin and palate. The calcium dependency index suggested that PAD activity was considerably dependent on calcium in the skin, but had small dependence in the oral mucosa, and activity was likely to be retained in the palate even in the presence of calcium concentrations as low

as 10 μM.

Detection of citrullinated proteins in stratified rat epithelial tissues

Figure 3A shows the immunoblot profiles upon probing with the anti-CPP antibody, which recognizes synthetic CCP originating from the primary structure of FLG. The major signal had an apparent molecular weight of 50 kDa. Immunoblots probed with anti-MC antibody, which recognizes citrulline residues after chemical modification, revealed a major band at 50 kDa and a strong smear signal in the upper region of the lane. Without the chemical modification, this antibody would not show reactivity. The intensity of these signals was in the descending order of skin > palate > buccal mucosa. Although citrullinated FLG and proFLG signals were likely present, other citrullinated proteins in the upper part of the lane and those at about 50–60 kDa, such as K1, should also be taken into account.

To discriminate between citrullinated keratins and FLG by protein charge, we performed 2D gel electrophoresis using NEpHGE in the first dimension and SDS-PAGE in the second dimension (Fig. 3B). Type I and type II keratins were acidic (isoelectric point [pI] = 4–5) and relatively basic (pI = 6–8), respectively, whereas FLG was a much more basic protein (pI = 10). The twin protein spots located around 50 kDa on the most cathodic side of the membrane were immunoreactive to anti-FLG antiserum. After the blot was stripped, we confirmed that there was no immunodetection of spots after incubation with the secondary antibody alone (data not shown). This suggests that no residual traces of bound FLG antibody immunoreacted with the spots. Re-probing of the blot with anti-CCP antibody revealed that FLG-immunoreactive spots included anti-CCP reactivity, suggesting that the FLG monomer was partly citrullinated in the skin (Fig. 3B). Total protein staining revealed multiple spots in the middle and anodic

side of the membrane, which likely included K1 and K10. Some of the spots (50 and 60 kDa) reacted positively with the anti-CCP antibody. In the palate, a small spot located around 50 kDa on the most cathodic side of the membrane also reacted with anti-FLG antiserum, although the signal was rather weak, so CCP immunoreactivity was not evident (Fig. 3B).

Co-existence of structural proteins and PAD in the cornified and granular layers of the skin and palatal mucosa

To determine the tissues where the structural proteins (FLG and K1) and PAD1 associated physically or functionally, we performed immunofluorescence experiments and viewed the images by confocal microscopy (Fig. 4). Signals for both FLG and K1 overlapped in the lower cornified layer of the skin. Pearson's colocalization coefficient was 0.96 in the cornified layer and 0.62 in the granular layer (squares in Fig. 4), suggesting the probable physical association of these proteins in KIFs. Merged localization was not observed in the palate or buccal mucosa (coefficients; 0.54 in the palate and 0.34 in the buccal mucosa). In both the skin and palatal mucosa, we observed the continuous immunofluorescence of PAD1 in the cornified layer, and a number of dot-like stains in the granular layer. Intense co-localization of PAD1 and K1 was detected in the cornified layer of the skin, suggesting that the chemical modification of K1 and probably FLG occurs in this tissue. However, such co-localization was not found in the superficial layers of the palatal mucosa. In the buccal mucosa, PAD localization was not observed.

Next, we immunostained the citrullinated proteins using anti-CCP antibody (Fig. 4) and observed an intense signal in the cornified layer of the skin, but a faint signal in the palatal and buccal mucosal layers. A considerable part of the K1 signal was merged

with the CCP signal, indicating that K1 and probably FLG are citrullinated in the cornified layer of the skin. The continuous MC staining in the cornified layer of skin was also merged with FLG staining. Scattered staining of MC and proFLG was found in the granular layer of the palate, some of which overlapped, indicating that proFLG may be citrullinated in keratohyalin granules (Fig. 4).

Organotypic culture models of rat palatal mucosa: Involvement of PAD in modification of FLG

Next, we analyzed the structure of the stratified layers during keratinization using reconstruction models (8 days after airlifting) derived from epithelial cells and fibroblasts isolated from the palatal mucosa of 7-day-old rats. As previously reported (14), the culture models retained their multi-layered epithelial structure with a cornified layer (Fig. 5A, control). The dot-like distribution of proFLG and diffusible localization of K1 were found in the granular layers. Similar to the *in vivo* palate preparation (see Fig. 4), the scattered staining of proFLG was merged with MC staining in the granular layer of the organotypic culture model (Fig. 5B, control).

Cl-amidine is a pan-inhibitor of PAD (24). We confirmed that this compound (10 μM) effectively reduced citrullination of histone H3 in the presence of hPAD4 using anti-MC antibody in immunoblot study (Fig. 5C). Cl-amidine significantly decreased PAD activity in rat palatal epithelial lysates and recombinant hPAD4 in the ABAP assay. In the presence of Cl-amidine, the reconstruction model appeared to be tightly overlaid with the cornified layer and the cells were flattened in the granular layer (Fig. 5A). Acefylline (100 μM), an activator of PAD1 and PAD3 (25), increased PAD activity of the rat palatal epithelium in the ABAP assay. The surface structure appeared to be looser and the cells exhibited minimal flattening (Fig. 5A).

We examined the effects of Cl-amidine and acefylline on the expression of FLG, K1, and citrullinated proteins in the reconstruction models. Neither Cl-amidine nor acefylline changed K1 immunostaining in the granular layer, but nonspecific staining was occasionally observed in some basal cells. Treatment with Cl-amidine resulted in continuous FLG staining in the cornified layers as well as granular proFLG staining (Fig. 5A, B). Interspersed co-localization was found in the confocal images of surface FLG and K1 immunoreactivity (Fig. 5B). Both continuous and granular FLG staining was negative to the anti-MC antibody. Acefylline did not cause apparent changes in FLG immunoreactivity (Fig. 5A). Some fine dots showed co-immunoreactivity with proFLG and MC (Fig. 5B). Immunoblot analysis showed that Cl-amidine significantly increased the FLG monomer signal (48 kDa) 2.5-fold, whereas acefylline tended to decrease the signal (Fig. 6A).

To examine whether PAD activity is involved in the epithelial structure, epithelial thickness was quantified in the presence or absence of Cl-amidine and acefylline. Cl-amidine significantly decreased epithelial thickness and the relative value of the cornified layer relative to the entire epithelial layer (Fig. 6B). Acefylline significantly increased epithelial thickness although relative thickness remained unchanged. Then we further investigated whether the change in PAD activity altered mucosal permeability. The fluorescence dye Lucifer yellow was applied to the surface of the models in the presence or absence of these compounds. The dye was allowed to penetrate the cornified layer and left to stain below the layer for 10 h. Cl-amidine significantly inhibited dye permeability whereas acefylline enhanced it (Fig. 6C).

Discussion

Processing of proFLG has several crucial roles in maintaining epidermal integrity

such as aligning KIFs, and controlling significant changes in cell shape and epidermal texture (4). Knockdown of FLG in the reconstructed epidermis or organotypic skin models by single hairpin RNA and small interference RNA technology was shown to disrupt the diffusion barrier in a dye penetration assay (26, 27). In flaky tail mice, which lack normal proFLG, barrier function was impaired (28). FLG-null (*Flg*$^{-/-}$) mice exhibited loss of keratin patterns and deficiency of barrier integrity (29). Transient overexpression of FLG resulted in collapse of the intermediate filament network (30, 31). Thus, the proFLG system should be distinct among epithelia types to provide suitable rigidity and permeability to the environment. This study demonstrated the diffuse localization of FLG in the cornified layer of the skin, but not in the palate or buccal mucosa of rats, whereas granular localization of proFLG was detected in the rat skin and palate. The distinct expression of FLG and proFLG in different epithelial types has also been previously reported in humans. Immunofluorescence with the antibody against (pro)FLG showed diffuse staining in the cornified layer of the human palate and scattered dot-like staining in the granular layer of the palate and buccal mucosa, suggestive of proFLG deposition in keratohyalin granules (15, 16). Immunoblot analysis showed that both the FLG monomer and proFLG were present in the palate, whereas only proFLG was found in the buccal mucosa (15). These results suggest some species-specific differences in FLG and proFLG expression in different parts of the oral mucosa.

PAD1 is distributed in all living layers of the human epidermis and in granular and weakly cornified layers of the mouse epidermis (11). Other PAD isozymes may also be involved in the granular and lower cornified layers, with some redundancy (5, 11). In this study, the relative expression level of PAD1 was highest in the rat palate, whereas that of PAD2, PAD3, and PAD4 was highest in the skin, indicative of some tissue-

specific PAD expression. Interestingly, the ABAP assay revealed that maximal PAD activity in the presence of 5 mM calcium was lower in the palate than in the skin, but the rank order of PAD activity reversed with decreasing concentrations of calcium, suggesting that calcium dependency is completely different between the two epithelial types. Notably, hPAD1 and hPAD3 were fully effective in catalyzing FLG citrullination at calcium concentrations less than 1.0 mM and 1.5 mM, respectively (8). In contrast, hPAD2 required more than 2.5 mM calcium to produce maximal activity in citrullinating FLG (8). Therefore, the high level of PAD1 in the palate allowed FLG citrullination even under low calcium concentrations. Because a gradient of calcium concentration has been reported in the epidermis (32), a relationship between intracellular calcium levels and the specific expression of the PAD isozymes with distinct calcium dependency in oral mucosa should be clarified in future studies.

FLG and K1 are preferentially citrullinated during the terminal differentiation of human epidermis (33). PAD1, but not other isozymes, is present in the uppermost cornified layer in the skin (8) and is responsible for K1 citrullination at this level (7, 10). FLG has been reported to be co-localized with PAD3 as well as PAD1 in the keratin matrix of lower cornified layer. In the human granular layer, proFLG has been shown to be co-localized with PAD1 and PAD3 on the granules; only PAD1 but not proFLG nor PAD3 were detected on the KIFs (8). The present study showed entirely distinct patterns of co-localization among the epithelial types in rats; FLG and K1 were co-localized with PAD1 in the cornified layers of skin, suggesting that FLG monomer and PAD may associate with KIFs and create tight bundles. However, neither FLG monomer nor K1 was co-expressed on the surface of the palate even though PAD1 was present (Fig. 7). Because of the granular presence of proFLG and PAD1, keratohyalin granules may be another place for citrullination by PAD1 in the palate, although other

protein substrates of PAD1, as yet uncharacterized, might be involved.

To determine where citrullinated proteins are localized in these epithelia, we took two approaches to detect the citrullination of FLG and keratins. It was reported that synthetic CCP originating from FLG recognized autoantibodies directed toward citrullinated protein generated in rheumatoid arthritis patients (34). This study used an anti-CCP antibody raised against cyclic synthetic peptide including citrulline residues within human FLG. This antibody likely recognized citrullinated FLG in our immunoblot and immunohistochemistry experiments. Furthermore, detection of the MC residues revealed the presence of citrullinated (pro)FLG (19). In our western blot analyses combined with 2D electrophoresis, the anti-CCP antibody was capable of detecting FLG monomer, whereas the anti-MC antibody likely detected proFLG, its processing intermediates, and the FLG monomer as well as all citrullinated proteins. The more intense FLG immunoreactivity in the three epithelial types and additional immunoreactive spots observed by 2D gel electrophoresis indicated the involvement of other citrullinated proteins such as K1, K10, and hornerin (35).

Our immunofluorescence studies revealed the overlapping surface distribution of K1, FLG, and CCP staining, suggesting that chemical modification of K1/FLG likely take places in the cornified layers of the skin. In the palate and its culture model, clear dot-like staining was observed in the immunofluorescent images for proFLG and MC, suggesting that chemical modification of proFLG is likely to be predominantly in keratohyalin granules, consistent with the previous notion of proFLG citrullination in keratohyalin granules (36–38). Loss of positive charges in proFLG could affect the integrity of the oral mucosa, for example, by altering the alignment of KIFs and changing the cell shape and mucosal texture (Fig. 7).

As mentioned above, the amount and type of PAD isozymes, their substrates, and

conditions of citrullination reactions were clearly distinct among the three epithelial types. To understand the precise role of PAD in the structure and function of oral mucosa, we attempted to make experimental conditions other than PAD activity the same using a rat 3D mucosal model and two types of compounds that are known to modify PAD. Cl-amidine inhibits the calcium-bound form of PADs and is the most widely used pan-PAD inhibitor in numerous disease models (24). As a PAD activator, xanthine derivative acefylline is useful for the citrullination of FLG by PAD1 and PAD3 (25). The present study revealed that PAD inhibition decreased the epithelium thickness and Lucifer yellow permeability concomitantly with an increase in expression of the FLG monomer. The fact that citrullination was lost in granular proFLG staining and that K1 and FLG monomer were co-expressed suggests that the persistent presence of FLG monomer may cause keratins to bundle tightly to make the epithelial compact in the PAD-deficient palate. On the other hand, further activation of PAD by acefylline in the palatal epithelium decreased expression of the FLG monomer, and increased the epithelium thickness and dye permeability. These data suggest that FLG citrullination contributes to the breakdown of (pro)FLG and the intrinsic structure of the oral mucosa to affect the barrier function. The present study strongly supports the notion that citrullinated filaggrin is involved in the function and morphology of stratified epithelia (10).

In conclusion, citrullination is likely to play an important role in maintaining structure and function of oral mucosa. The results of this study provide new insights into the complex mechanism underlying the cornification and stratification of epithelium in the oral mucosa, and paves the way for new pharmacological approaches directed toward the maintenance of sustainable oral health.

Acknowledgments

We thank Dr. Akihito Ishigami for his gift of the anti-FLG antiserum. Dr. Kenichi Kato is acknowledged for helpful discussions. This work was supported by JSPS KAKENHI (Grant-in-Aid for Scientific Research, Grant Number JP26670104). The authors report no conflicts of interest related to this study.

References

1. Vossenaar ER, Zendman AJ, van Venrooij WJ, Pruijn GJ. PAD, a growing family of citrullinating enzymes: genes, features and involvement in disease. Bioessays 2003; 25: 1106-1118.
2. Sandilands A, Sutherland C, Irvine AD, McLean WH. Filaggrin in the frontline: role in skin barrier function and disease. J Cell Sci 2009; 122: 1285-1294.
3. Dale BA, Holbrook KA, Steinert PM. Assembly of stratum corneum basic protein and keratin filaments in macrofibrils. Nature 1978; 276: 729-731.
4. Candi E, Schmidt R, Melino G. The cornified envelope: a model of cell death in the skin. Nat Rev Mol Cell Biol 2005; 6: 328-340.
5. Ishigami A, Asaga H, Ohsawa T, Akiyama K, Maruyama N. Peptidylarginine deiminase type I, type II, type III and type IV are expressed in rat epidermis. Biomed. Res 2001; 22: 63-65.
6. Ishigami A, Kuramoto M, Yamada M, Watanabe K, Senshu T. Molecular cloning of two novel types of peptidylarginine deiminase cDNAs from retinoic acid-treated culture of a newborn rat keratinocyte cell line. FEBS Lett 1998; 433: 113-118.
7. Senshu T, Akiyama K, Ishigami A, Nomura K. Studies on specificity of peptidylarginine deiminase reactions using an immunochemical probe that recognizes an enzymatically deiminated partial sequence of mouse keratin K1. J Dermatol Sci 1999; 21: 113-126.
8. Méchin MC, Enji M, Nachat R, et al. The peptidylarginine deiminases expressed in human epidermis differ in their substrate specificities and subcellular locations. Cell Mol Life Sci 2005; 62: 1984-1995.
9. Ishida-Yamamoto A, Senshu T, Takahashi H, Akiyama K, Nomura K, Iizuka H. Decreased deiminated keratin K1 in psoriatic hyperproliferative epidermis. J Invest

Dermatol 2000; 114: 701-705.

10. Ishida-Yamamoto A, Senshu T, Eady RA, et al. Sequential reorganization of cornified cell keratin filaments involving filaggrin-mediated compaction and keratin 1 deimination. J Invest Dermatol 2002; 118: 282-287.
11. Nachat R, Méchin MC, Takahara H, et al. Peptidylarginine deiminase isoforms 1-3 are expressed in the epidermis and involved in the deimination of K1 and filaggrin. J Invest Dermatol 2005; 124: 384-393.
12. Presland RB, Jurevic RJ. Making sense of the epithelial barrier: what molecular biology and genetics tell us about the functions of oral mucosal and epidermal tissues. J Dent Educ 2002; 66: 564-574.
13. Dale BA, Thompson WB, Stern IB. Distribution of histidine-rich basic protein, a possible keratin matrix protein, in rat oral epithelium. Arch Oral Biol 1982;27:535-545.
14. Murakami H, Okamura K, Aoki S, Sakagami R, Yamazaki J. Association of caspase-14 and filaggrin expression with keratinization of the oral mucosa and reconstruction culture rat models. J Periodontal Res 2014; 49: 703-710.
15. Smith SA, Dale BA. Immunologic localization of filaggrin in human oral epithelia and correlation with keratinization. J Invest Dermatol 1986; 86: 168-172.
16. Reibel J, Clausen H, Dale BA, Thacher SM. Immunohistochemical analysis of stratum corneum components in oral squamous epithelia. Differentiation 1989; 41: 237-244.
17. Makino T, Mizawa M, Inoue S, Noguchi M, Shimizu T. The expression profile of filaggrin-2 in the normal and pathologic human oral mucosa. Arch Dermatol Res 2016; 308: 213-217.
18. Larsen KR, Johansen JD, Reibel J, Zachariae C, Rosing K, Pedersen AML.

Filaggrin gene mutations and the distribution of filaggrin in oral mucosa of patients with oral lichen planus and healthy controls. J Eur Acad Dermatol Venereol 2017; 31: 887-893.

19. Senshu T, Akiyama K, Kan S, Asaga H, Ishigami A, Manabe M. Detection of deiminated proteins in rat skin: probing with a monospecific antibody after modification of citrulline residues. J Invest Dermatol 1995; 105: 163-169.
20. O'Farrell PZ, Goodman HM, O'Farrell PH. High resolution two-dimensional electrophoresis of basic as well as acidic proteins. Cell 1977; 12: 1133-1141.
21. Zendman AJ, Raijmakers R, Nijenhuis S, et al. ABAP: antibody-based assay for peptidylarginine deiminase activity. Anal Biochem 2007; 369: 232-240.
22. Okazaki M, Yoshimura K, Suzuki Y, Harii K. Effects of subepithelial fibroblasts on epithelial differentiation in human skin and oral mucosa: heterotypically recombined organotypic culture model. Plast Reconstr Surg 2003; 112: 784-792.
23. Dongari-Bagtzoglou A, Kashleva H. Development of a highly reproducible three-dimensional organotypic model of the oral mucosa. Nat Protoc 2006; 1: 2012-2018.
24. Witalison EE, Thompson PR, Hofseth LJ. Protein arginine deiminases and associated citrullination: Physiological functions and diseases associated with dysregulation. Curr Drug Targets 2015; 16: 700-710.
25. Méchin MC, Cau L, Galliano MF, et al. Acefylline activates filaggrin deimination by peptidylarginine deiminases in the upper epidermis. J Dermatol Sci 2016; 81: 101-106.
26. Mildner M, Jin J, Eckhart L, et al. Knockdown of filaggrin impairs diffusion barrier function and increases UV sensitivity in a human skin model. J Invest Dermatol 2010; 130: 2286-2294.
27. Pendaries V, Malaisse J, Pellerin L, et al. Knockdown of filaggrin in a three-

dimensional reconstructed human epidermis impairs keratinocyte differentiation. J Invest Dermatol 2014; 134: 2938-2946.

28. Presland RB, Boggess D, Lewis SP, Hull C, Fleckman P, Sundberg JP. Loss of normal profilaggrin and filaggrin in flaky tail (ft/ft) mice: an animal model for the filaggrin-deficient skin disease ichthyosis vulgaris. J Invest Dermatol 2000; 115: 1072-1081.
29. Kawasaki H, Nagao K, Kubo A, et al. Altered stratum corneum barrier and enhanced percutaneous immune responses in filaggrin-null mice. J Allergy Clin Immunol 2012; 129: 1538-1546.
30. Dale BA, Presland RB, Lewis SP, Underwood RA, Fleckman P. Transient expression of epidermal filaggrin in cultured cells causes collapse of intermediate filament networks with alteration of cell shape and nuclear integrity. J Invest Dermatol 1997; 108: 179-187.
31. Presland RB, Kuechle MK, Lewis SP, Fleckman P, Dale BA. Regulated expression of human filaggrin in keratinocytes results in cytoskeletal disruption, loss of cell-cell adhesion, and cell cycle arrest. Exp Cell Res 2001; 270: 199-213.
32. Celli A, Sanchez S, Behne M, Hazlett T, Gratton E, Mauro T. The epidermal Ca^{2+} gradient: Measurement using the phasor representation of fluorescent lifetime imaging. Biophys J 2010; 98: 911-921.
33. Senshu T, Kan S, Ogawa H, Manabe M, Asaga H. Preferential deimination of keratin K1 and filaggrin during the terminal differentiation of human epidermis. Biochem Biophys Res Commun 1996; 225: 712-719.
34. Schellekens GA, Visser H, de Jong BA, et al. The diagnostic properties of rheumatoid arthritis antibodies recognizing a cyclic citrullinated peptide. Arthritis Rheum 2000; 43: 155-163.

35. Hsu CY, Gasc G, Raymond AA, et al. Deimination of Human Hornerin Enhances its Processing by Calpain-1 and its Cross-Linking by Transglutaminases. J Invest Dermatol 2017;137:422-429.
36. Sebbag M, Simon M, Vincent C, et al. The antiperinuclear factor and the so-called antikeratin antibodies are the same rheumatoid arthritis-specific autoantibodies. J Clin Invest 1995; 95: 2672-2679.
37. Girbal-Neuhauser E, Montézin M, Croute F, et al. Normal human epidermal keratinocytes express in vitro specific molecular forms of (pro)filaggrin recognized by rheumatoid arthritis-associated antifilaggrin autoantibodies. Mol Med 1997; 3: 145-156.
38. Méchin MC, Sebbag M, Arnaud J, et al. Update on peptidylarginine deiminases and deimination in skin physiology and severe human diseases. Int J Cosmet Sci 2007; 29: 147-168.

Figure Legends

Fig. 1 Histological and immunofluorescence examination of the skin, palate, and buccal mucosa in 7-day-old rats. A, Hematoxylin and eosin staining (upper) and profilaggrin (proFLG) immunofluorescence using anti-filaggrin (FLG) antiserum (middle and lower). The arrowheads indicate keratohyalin granules (upper) and dot-like immunoreactivity for proFLG (lower). The squares a, b, and c are enlarged in the lower panels. Purple: DAPI staining. Broken line indicates the basement membrane. Dotted line indicates the surface of the epithelium. B, Quantitative analysis of relative area of the proFLG immunofluorescence. **P < 0.01; one-way analysis of variance followed by the *post hoc* Dunnett's test (n = 4). C, A representative image of immunoblot for proFLG protein. P, I, F, and D denote proFLG (~400 kDa), the processing intermediates of proFLG, FLG monomers (~48 kDa), and the degradation products of the monomers, respectively. Expression of β-actin is shown as a loading control.

Fig. 2 Expression of peptidylarginine deiminase (PAD) and filaggrin in the skin, palate, and buccal mucosa of rats. A, Typical real-time PCR results obtained using cDNA derived from three types of epithelial tissues and whole skin with specific primer pairs for PAD1–4 and GAPDH. B, Typical real-time PCR results and quantitative PCR data obtained using primer pairs for profilaggrin (proFLG) (n = 4 animals per group). C, Quantitative real-time PCR measurements of PAD1, PAD2, PAD3, and PAD4 mRNA are shown (n = 4 animals per group). Expression values were calculated by the relative standard curve method. *P < 0.05, **P < 0.01, ***P < 0.001; one-way analysis of variance followed by the *post hoc* Dunnett's *t*-test. D, PAD specific activity was measured in the presence of 10 μM, 100 μM, and 5 mM Ca^{2+} (antibody-based assay for PAD activity assay) using lysate (1 μg) obtained from 3 epithelial types (n = 3–4) (left).

The ratio of PAD activity in 5 mM Ca^{2+} to that in 10 μM Ca^{2+} is shown to clarify the distinct calcium dependency among the three. *P < 0.05, **P < 0.01, ***P < 0.001; one-way analysis of variance followed by the *post hoc* Bonferroni's *t*-test.

Fig. 3 Separation of citrullinated protein in the skin, palate, and buccal mucosa of rats. A, immunoblot following 4–20% gradient sodium dodecyl sulfate-polyacrylamide gel electrophoresis (SDS-PAGE) using anti-cyclic citrullinated peptide (CCP) and anti-modified citrulline (MC) protein antibodies. Immunoreactivity of anti-MC antibody with or without citrulline modification of the skin sample is also shown. Expression of β-actin is shown as a loading control. B, Two-dimensional profiles of immunoblot using anti-filaggrin (FLG) antiserum and anti-CPP antibody. The samples were loaded on agarose gels, separated in the first dimension using NEpHGE, and separated in the second dimension by SDS-PAGE. FLG: immunodetection of (pro)FLG. CCP: immunodetection of citrullinated protein. Merged skin and palate: images obtained by superimposing total protein (colloidal gold) with (pro)FLG (green) and the citrullinated proteins (red).

Fig. 4 Immunofluorescence images for expression of (pro)filaggrin [(pro)FLG], peptidylarginine deiminase (PAD)1, and citrullinated proteins in the skin, palate, and buccal mucosa of rats under a confocal microscope. For detection of the citrullinated proteins, anti-cyclic citrullinated peptide (CCP) antibody and anti-modified citrulline (MC) antibody were used. (G): green. (R): red. Yellow staining denotes the overlapping signals. Squares are enlarged in the lower panels. Arrowheads indicate the dot-like immunoreactivity for proFLG and MC. Purple: DAPI staining. Broken line indicates the basement membrane. Dotted line indicates the surface of the epithelium.

Fig. 5 Organotypic reconstruction models using epithelial cells and fibroblasts dissociated from rat palatal mucosa. The models were cultured in the presence or absence of a pan- peptidylarginine deiminase (PAD) inhibitor Cl-amidine (10 μM) or acefylline (100 μM) for 5 days. A, Hematoxylin and eosin (H&E) staining and immunofluorescence using anti-filaggrin (FLG) antiserum in the reconstruction models. The squares are enlarged. Arrowheads denote granular presence of profilaggrin (proFLG). Broken line indicates the basement membrane. B, Confocal images using anti-FLG antiserum, anti-keratin 1 (K1), and anti-modified citrulline (MC) antibodies in the reconstruction models. (G): green. (R): red. Yellow staining (arrows) denotes the overlapping granular signals. Dotted line indicates the surface of the epithelium. C, Validity of Cl-amidine and acefylline in modulating PAD activity was tested. Immunoblotting using anti-MC antibody was performed in the presence of recombinant human PAD4 (hPAD4) and histone H3 as a substrate with or without Cl-amidine. An antibody-based assay for PAD activity assay to check the validity of Cl-amidine and acefylline was also performed using hPAD4 and rat palatal epithelial lysate (n = 3). PAD specific activity was measured in the presence of 5 mM Ca^{2+} using lysate (1 μg) obtained from rat palatal epithelium.

Fig. 6 Quantitative analysis of epithelial structure and expression pattern of filaggrin (FLG) in the reconstruction models treated for 5 days with or without Cl-amidine (10 μM) or acefylline (100 μM). A, Immunoblot using anti-FLG antiserum (upper). Quantitative measurement of FLG monomer (48 kDa, closed triangle) is shown (n = 4) (lower). Expression of β-actin is shown as a loading control. B, Thickness of all epithelial layers (upper) and relative thickness of the cornified layer with respect to all

epithelial layers (lower) (n = 6). C, Permeability to lower epithelium with Lucifer yellow applied onto the surface of the palate models. After 10 h, the models were fixed. Permeability index was calculated using fluorescence intensity within the noncornified area (surrounded by broken lines) (n = 3). *P < 0.05, **P < 0.01, ***P < 0.001; one-way analysis of variance followed by *post hoc* Bonferroni's *t*-test.

Fig. 7 Schematic models of enzymatic breakdown of profilaggrin (proFLG) in rat skin and palate. ProFLG is stored in keratohyalin granules of the granular layer. ProFLG is proteolyzed to FLG monomers which associate with keratin intermediate filaments (KIF) in the cornified layer of the skin. Peptidylarginine deiminase (PAD) including PAD1 is co-localized in KIF and/or keratohyalin granules, and is likely to citrullinate FLG or proFLG (denoted as open marks) and to decrease the intermolecular interaction resulting in proteolytic degradation. PAD3 may be involved in protein citrullination in skin (8). The pattern of proFLG breakdown in the palate is likely to be distinct from that in the skin.

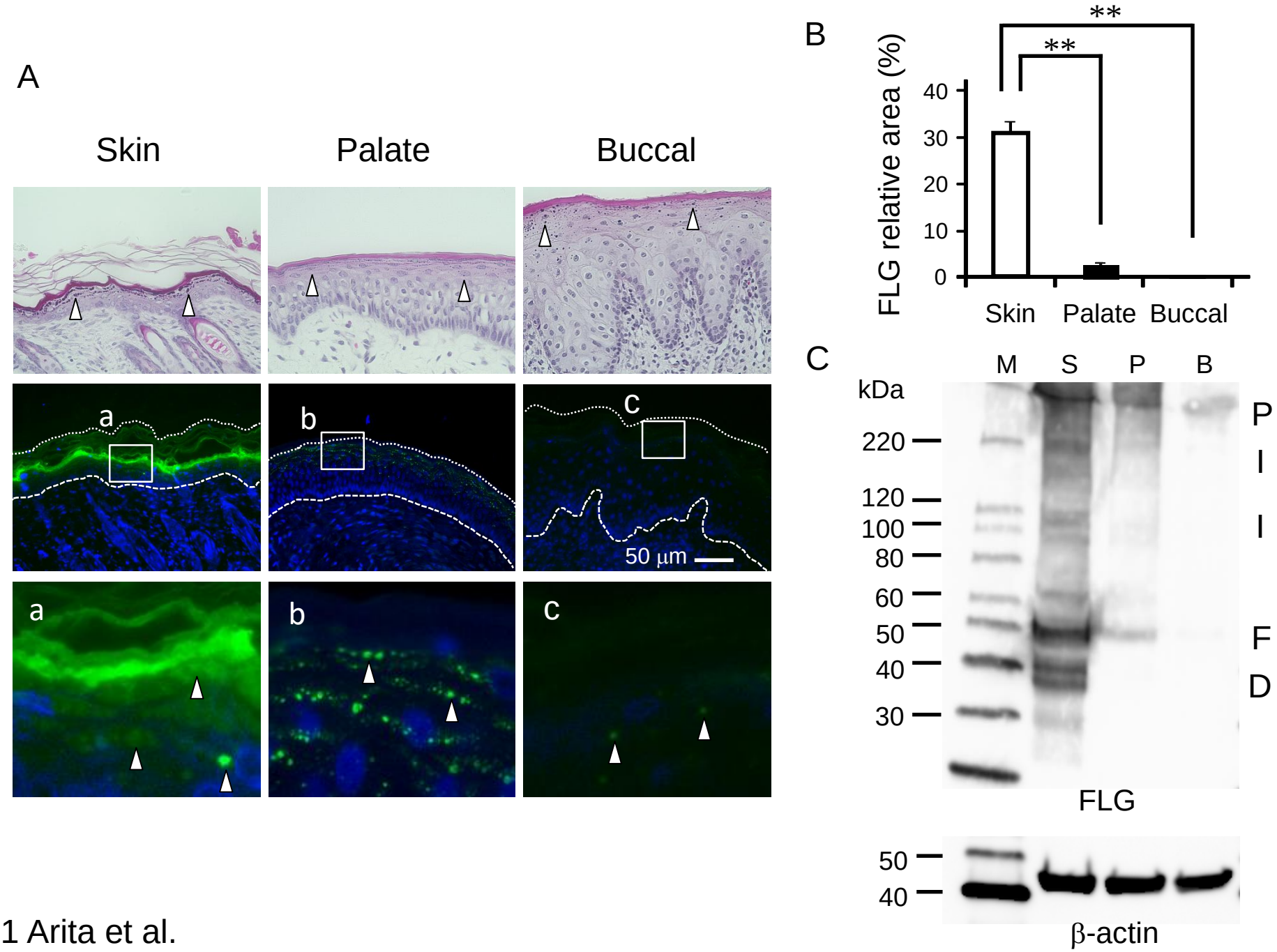

Fig.1 Arita et al.

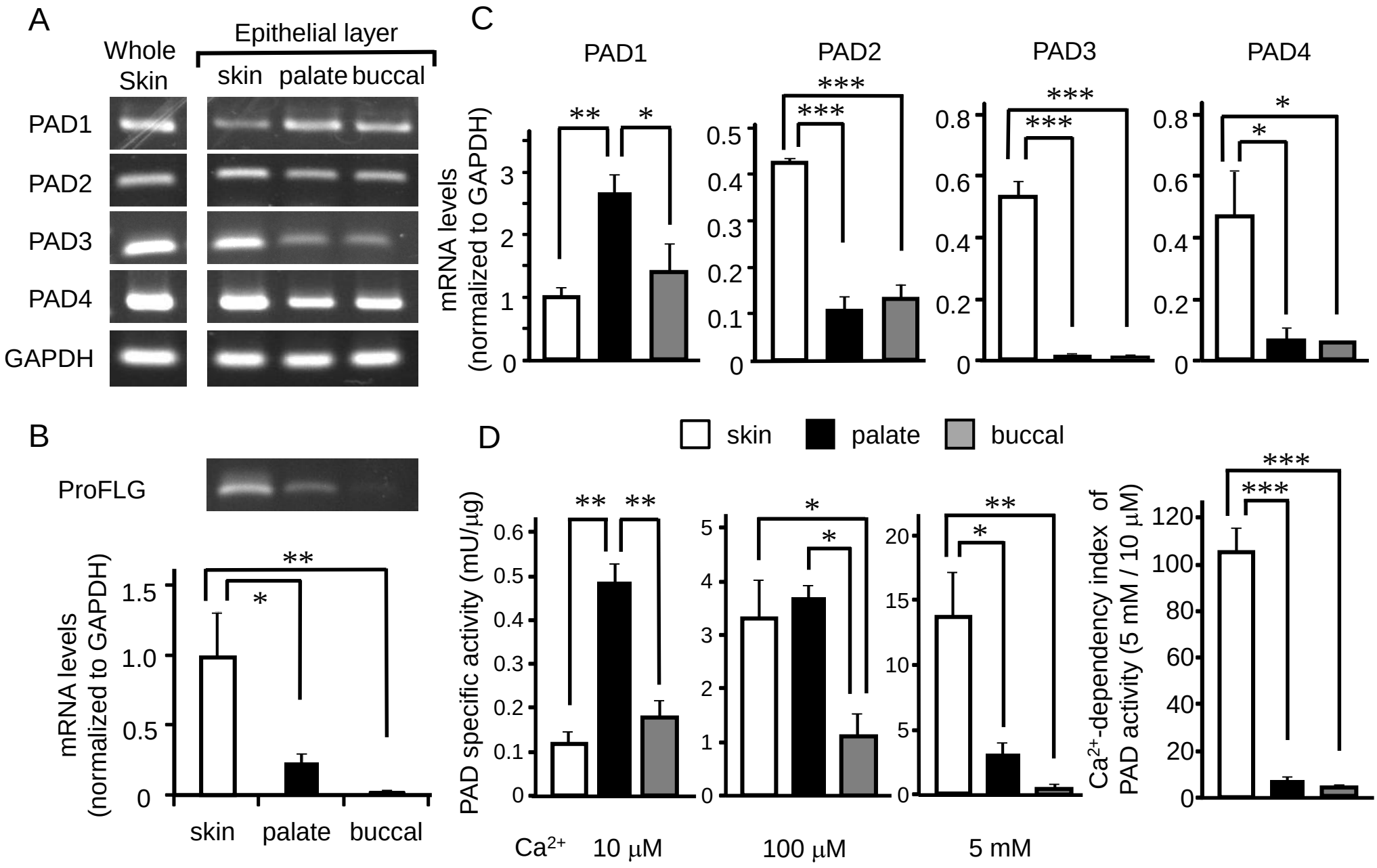

Fig.2 Arita et al.

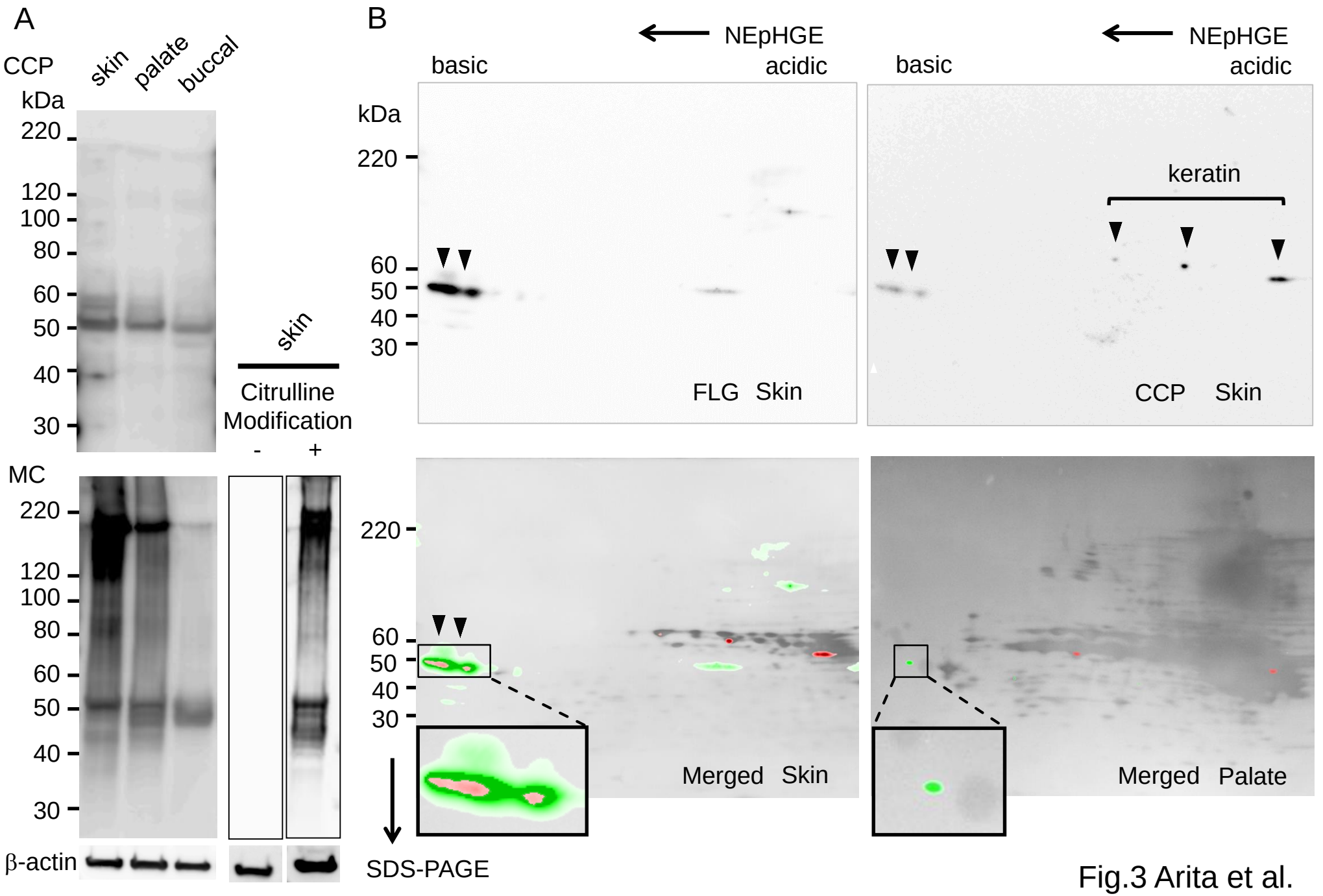

Fig.3 Arita et al.

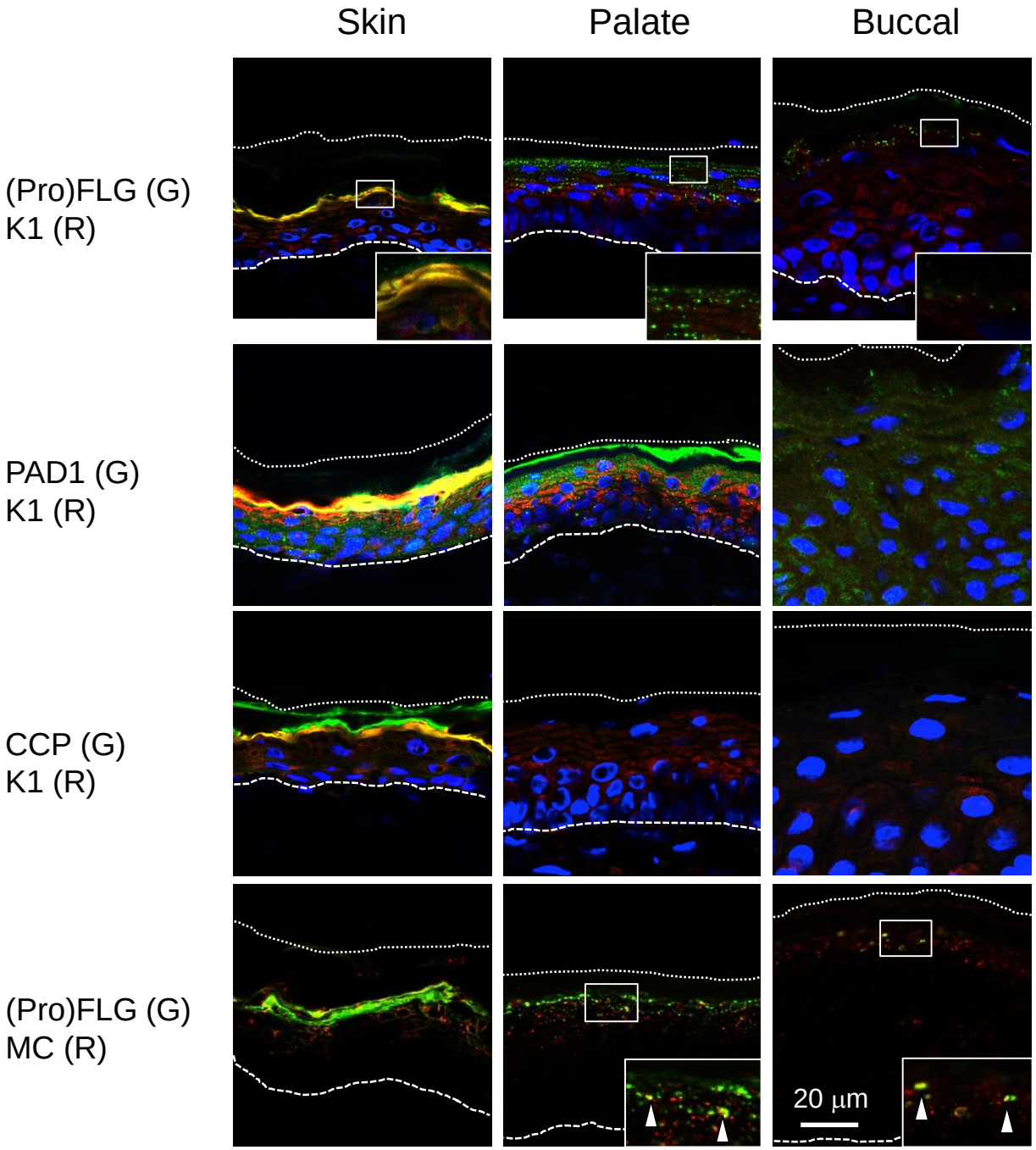

Fig.4 Arita et al.

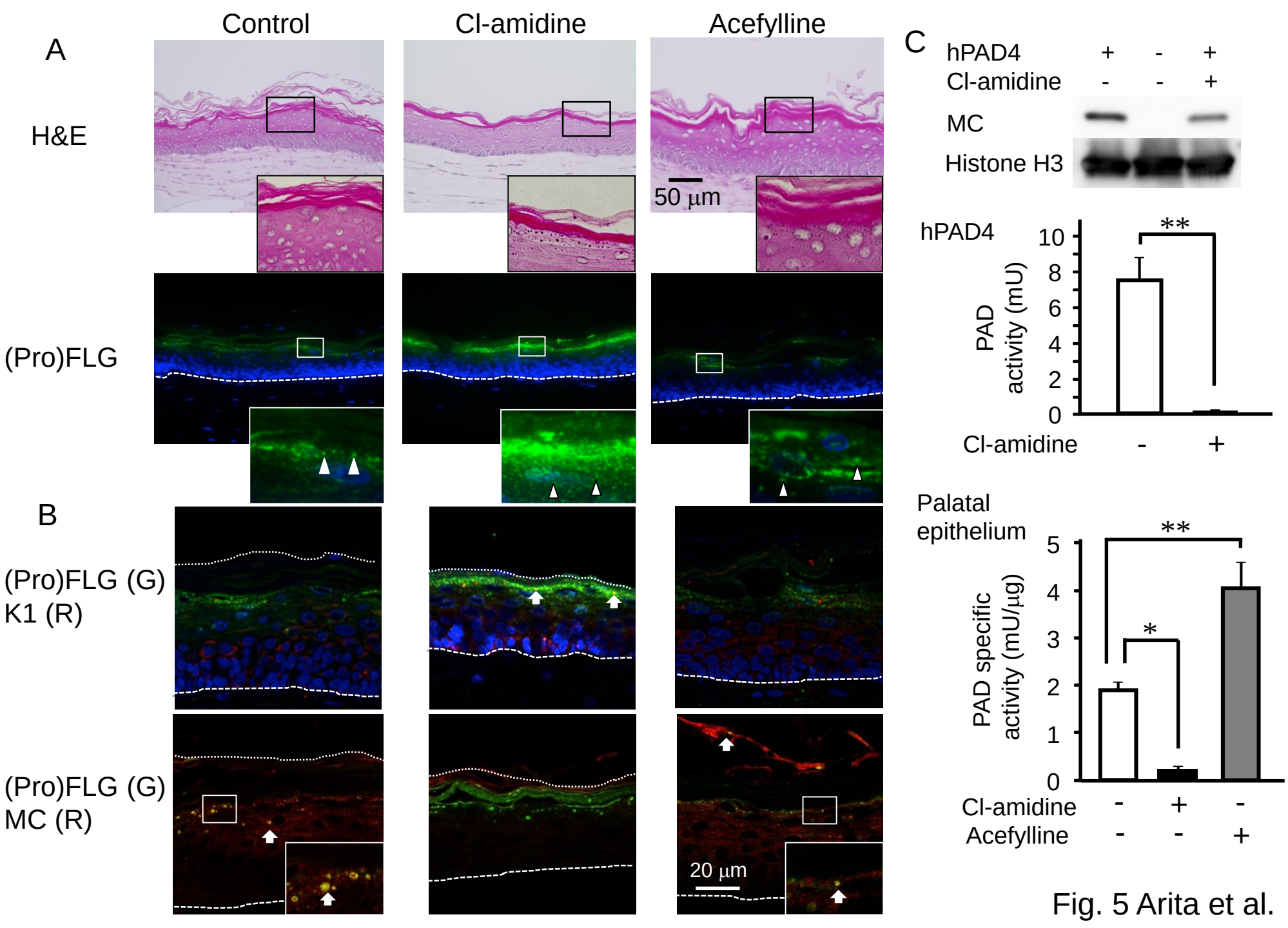

Fig. 5 Arita et al.

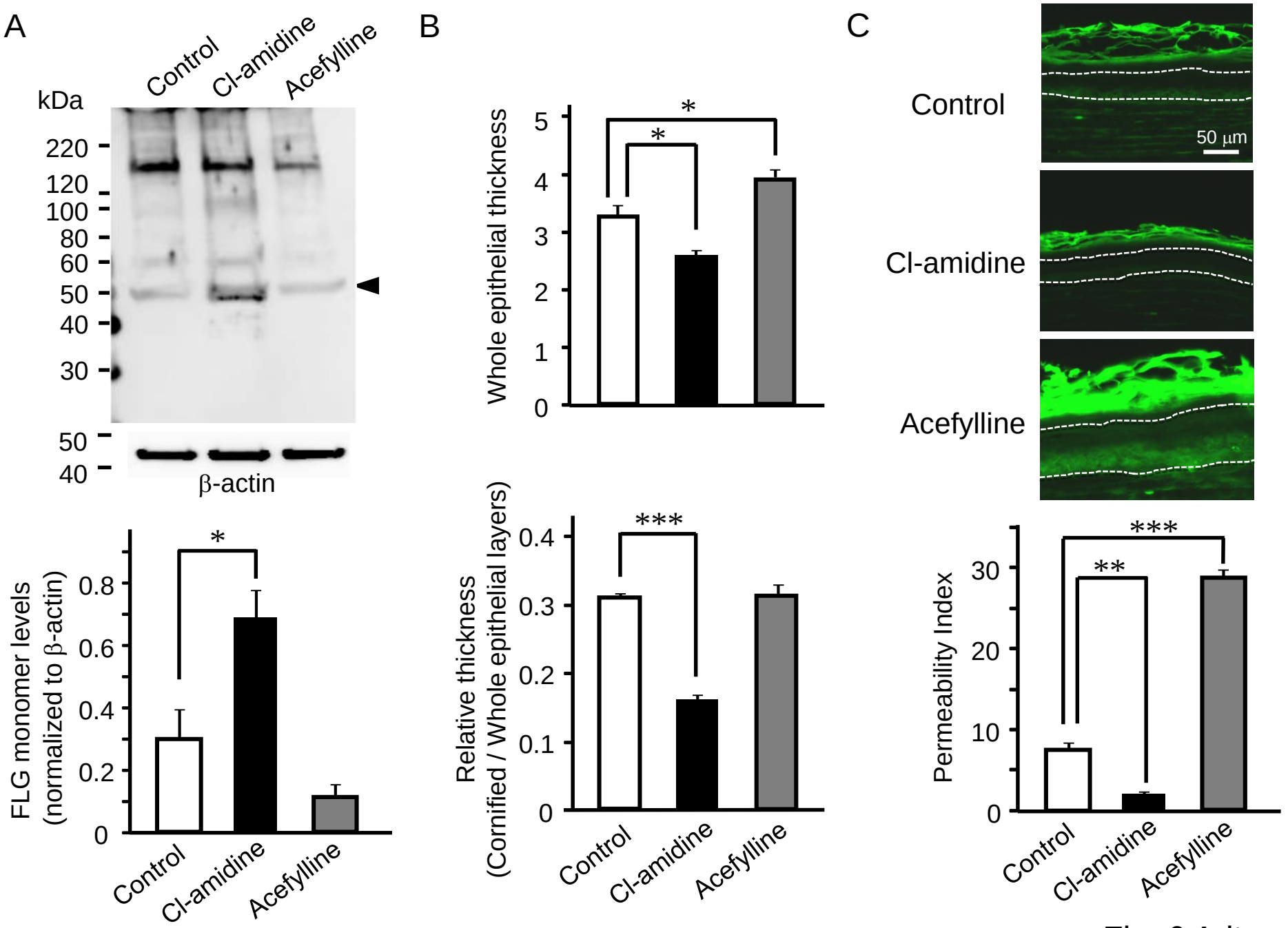

Fig. 6 Arita et al.

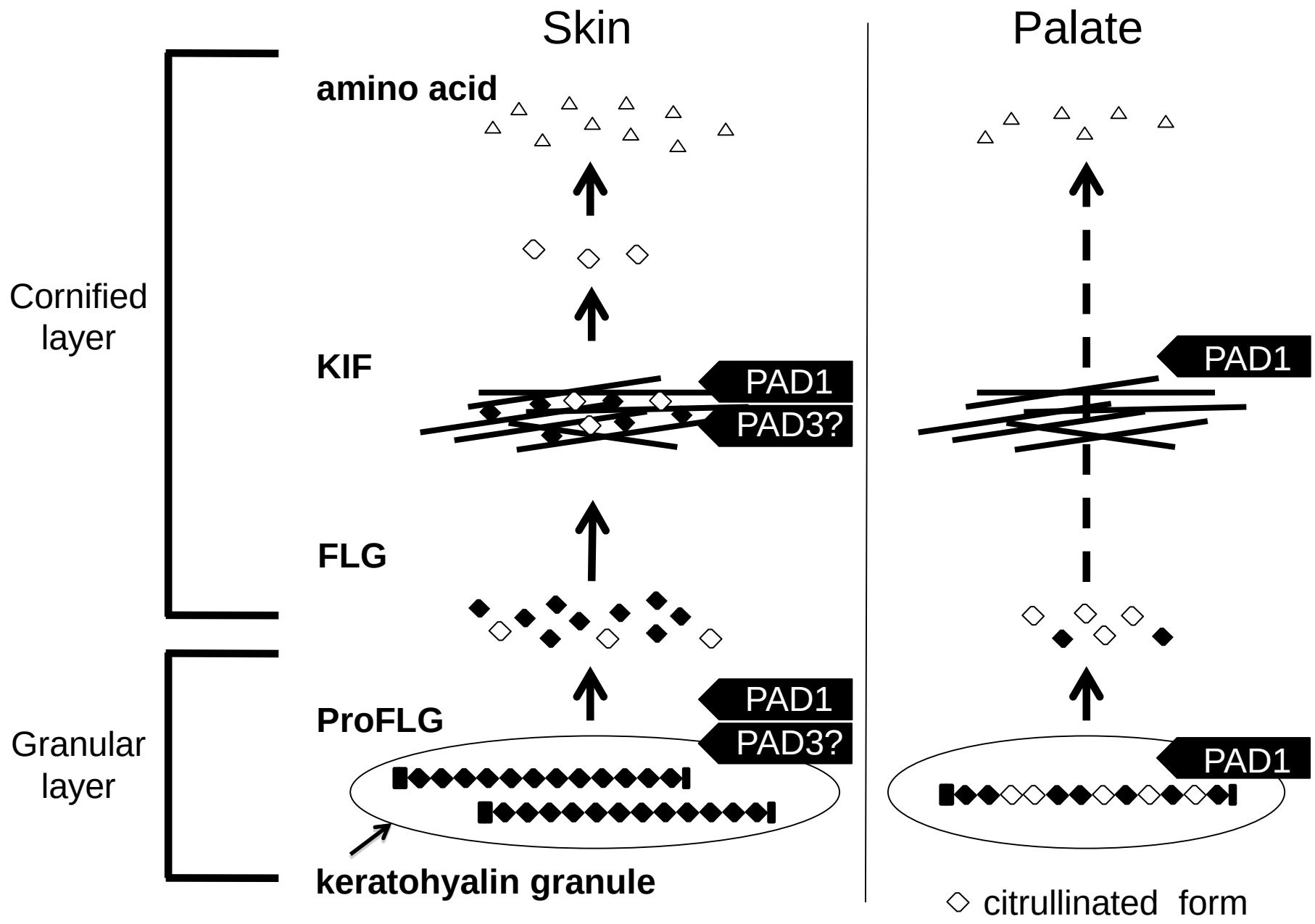

Fig. 7 Arita et al.